www.sensorsportal.com

Sensors & Transducers

Published by IFSA Publishing, S. L., 2020
http://www.sensorsportal.com

Advanced Measurement Procedure for Interferometric Microscope for Three-dimensional Imaging of Complex Surfaces Using Two-wavelength Interferometry and Reference Arm Attenuation

[1,*] Marek Stašík, [1] František Kaván, [2] Marek Mach, [1] Karolína Sedláčková, [1] Jan Kredba and [2] Michal Špína

[1] Technical University of Liberec, Institute of New Technologies and Applied Informatics, Studentská 1402/2, 461 17 Liberec, Czech Republic

[2] Regional Centre for Special Optics and Optoelectronic Systems (TOPTEC), Institute of Plasma Physics, Academy of Sciences of the Czech Republic, Za Slovankou 1782/3, 182 00 Prague 8, Czech Republic

[*] Tel.: 420604534584

[*] E-mail: marek.stasik@tul.cz

Received: 30 October 2020 /Accepted: 30 November 2020 /Published: 31 December 2020

Abstract: Digital holographic microscopy is a powerful 3D imaging tool for industrial surface inspection and scientific experiment evaluation, as it provides lateral resolution similar to classical microscopy and very fine axial resolution. This paper presents the results and the findings of experimental holographic microscope development. The device construction is described. The research emphasises on two-wavelength interferometry combined with phase shifting. The phase shifting was done using acousto-optic modulators, which allow precise tuning of light frequency. A developed enhanced measurement procedure which increases versatility by increasing dynamic range is described. Developed algorithms for data evaluation are presented and measured experimental data visualised.

Keywords: Microscope, Interferometry, Phase shifting, Bragg cell, Acousto-optic modulator, Multiwavelength interferometry, High dynamic range.

1. Introduction

Microscopy is the standard inspection method for surface quality evaluation. One of the disadvantages of classical microscopy is the ability to sense only light intensity, so it can only be used to gather 2D information about the object. To gather 3D or phase information about the object we can use digital holographic microscopy (DHM). A digital holographic microscope introduces the possibility to precisely measure surface height with axial resolution of about 30 nm [1]. Lateral resolution of DHM is similar to the conventional optical microscope. With the correct adjustment it reaches sub-micrometre resolution. The fundamental construction of the holographic microscope is similar to the standard optical microscope. The main difference is that the holographic microscope uses a coherent light source, and a reference wavefront is introduced to a detector. Then interference pattern of those two wavefronts is recorded and evaluated [2].

To be able to measure phase distribution in this in-line arrangement, it is necessary to implement some form of controlled phase shifting. In this microscope a phase difference between the object and reference wavefront is controlled with the acousto-optic modulators (AOM) and the interference patterns are captured for various phase differences. Two different approaches were examined. First possibility is to use slightly different carrier frequencies (e.g. 80 MHz, 80.000001 MHz – 1 Hz difference), which cause the interference pattern to periodically change with frequency equal to the frequency difference of those carrier frequencies. With the right sampling rate, it is possible to get frames with exact phase differences. Second method is to use the same carrier frequencies and change their phase difference, which causes the same phase shift in the interference pattern. While the first method is much faster, it causes the interference pattern to blur, decreasing precision. So, when the signal is low and higher exposure times need to be used, it is preferable to choose discrete phase steps rather than continuous sweep [1, 3].

Most digital holographic microscopes work in transmission mode, where the phase mostly corresponds to refractive index variations [1]. However, for topography measurement and especially with the opaque objects, this approach cannot be used. So, the microscope has to work in reflection mode. This geometry allows for topography measurement of objects such as microelectromechanical structures (MEMS) with high degree of precision, almost in real time [2, 3]. Inspection of a discontinuous surface with significant steps or surfaces with non-specular reflection is problematic when simple interferometry is used, due to discontinuous phase distribution and speckle noise. To overcome this issue, two wavelength approach can be used. This method uses two recording wavelengths instead of one. It decreases the overall precision, but allows the measurement of those diffuse objects, that would otherwise be impossible to be measured by standard single wavelength method [4]. Those two wavelength holograms are captured subsequently, and their phase is then subtracted. It creates another phase field called synthetic phase field and its measure is synthetic wavelength $\Lambda \approx \lambda 2/\Delta\lambda$. This synthetic wavelength can be tuned by adjusting the wavelength difference, so that it is ideal for the measured object, it is always larger than laser wavelength, therefore the decreased precision, but increased range.

Phase shifting is a reliable method when all parts of the measured surface reflect a similar amount of light. When the surface contains parts where there is significantly less light reflected, it reduces the modulation amplitude, which negatively impacts the signal-to-noise ratio, making the phase-shifting less precise or even impossible. In order to compensate for this difference, a high dynamic range (HDR) approach was proposed and tested. The intensity of reference wave and the exposure time of the camera can be altered to get the best modulation from different parts of the surface. This method is an extension of the method that is widely used in conventional photography [4, 5].

The main aim of this work is to use an experimental digital holographic microscope and test the mentioned improvement methods in the practical measurement of samples related to industrial production. As a test specimen a piece of printed circuit board (PCB) was used as it has challenging properties for this type of measurement.

This paper is based on previous conference paper [6].

2. Phase Shifting

A standard holographic measurement approach uses phase shifting to solve the problem of the unknown light intensity offset and gain. A few methods can be used to introduce phase shifting to the system. The developed experimental microscope setup uses a set of two fibre acousto-optic modulators – so-called Bragg cells – in the reference and the illumination-object arm. These modulators are driven by an alternating electrical signal. The frequency and phase of the output light frequency shift is equal to the electrical signal frequency and phase. The acousto-optic modulators work at a frequency in the order of tens of MHz. The difference of the frequencies can be arbitrarily small, for example, units of Hz.

As a result of the frequency difference, time dependent phase shifting is introduced between the object and the reference wavefront.

$$\hat{\mathrm{E}}_{\mathrm{ref}}(t) = A \cdot |\hat{E}_{in}| \cdot e^{i \cdot t \cdot (\omega_0 + \omega_{ref})} \quad (1)$$

$$\hat{\mathrm{E}}_{\mathrm{obj}}(t) = A \cdot |\hat{E}_{in}| \cdot e^{i \cdot t \cdot (\omega_0 + \omega_{obj})} \quad (2)$$

In equations (1) and (2), there are the prescriptions of the output wave of the acousto-optics modulators in the reference and in the object arm. The value A is the amplification of the modulator and the value $|E_{\mathrm{in}}|$ is the amplitude of the input wave. The functions are complex and are dependent on the time t. The value ω_0 represents the angular frequency of the input light and the values ω_{ref} and ω_{obj} represent the angular frequencies of the control signal driving each modulator.

$$\delta(t) = t \cdot (\omega_0 + \omega_{ref}) - t \cdot (\omega_0 + \omega_{obj}) \quad (3)$$

$$\delta(t) = t \cdot (\omega_{obj} - \omega_{ref}) \quad (4)$$

The phase difference δ(t) in expression (3) is then a function of the time t. It can be simplified to function (4).

The detected intensity in one pixel for discrete number of samples can be described by expression (5).

$$I_i = I_A \cdot \sin(\delta_i + \Delta\phi) + I_{offset} \\ \delta_i = \delta(t_i) \quad (5)$$

Variable I_i represent intensity on the detector. Variable I_A represents amplitude of the sinus function. Variable δ_i is the introduced phase shift. Variable $\Delta\phi$ is the phase of the object to be measured. Variable I_{offset} is the intensity offset of the sinus function. Index i represent index of the sample.

The principle of the phase shift evaluation is visualized in Fig. 1.

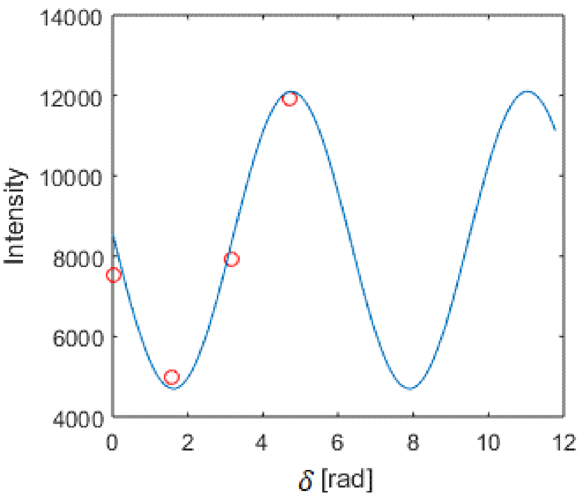

Fig. 1. Visualization of the fitting of four measured intensities in one pixel by the sinus function.

There are various methods how the sinus function fitting can be done. The main goal of the fitting is to obtain the value $\Delta\phi$ for each pixel. This phase value can be converted to the optical path difference.

2.1. Four Steps Algorithm

A sequence of four frames is taken. Since the time of each frame is known, the introduced phase shift can be calculated from function (4). For each pixel in the images, four irradiance values I_1, I_2, I_3 and I_4 are, therefore, known. Considering the phase step between each shot is $\pi/2$, formula (6) can be used to calculate the detected phase $\Delta\phi$ in each pixel [8].

$$\Delta\phi = \arctan\left(\frac{I_4 - I_2}{I_1 - I_3}\right) \quad (6)$$

The values of the $\Delta\phi$ form a phase map. The resulting phase map is wrapped and it has to be unwrapped. The advantage of this method is that, it is based on the analytical formula and it is not iterative algorithm.

2.2. Thirteen Steps Algorithm

This algorithm is similar to the four step algorithm. It provides phase values by an analytical formula as the four step algorithm does. The analytical formula is in expression (7).

$$\hat{U} = \big(3 \cdot (I_1 - I_{13}) + 4 \cdot (I_2 - I_{12}) - 12 \cdot (I_4 - I_{10}) \\ - 21 \cdot (I_5 - I_9) - 16 \cdot (I_6 - I_8)\big) \\ + (4 \cdot (I_2 + I_{12}) + 12 \\ \cdot (I_3 + I_{11} + I_4 + I_{10}) - 16 \\ \cdot (I_6 + I_8) - 24 \cdot I_7) \cdot i \quad (7)$$

The character i in the expression is complex unit. Output of the formula is complex number, so it is able to provide information about phase and amplitude of the modulated sinus wave. The condition of this method is equidistant spacing between each phase shift $\pi/4$. Nevertheless this algorithm is not as much sensitive to the deviation from optimal phase step as the four step algorithm.

2.3. Iterative Least Square Fitting

This method is preferable when phase shift values of each sample are known with a significant amount of uncertainty. Each iteration of this algorithm can be divided to the two stages. In the first stage, it converts the problem to the system of linear equations and uses least square method to find phase value for each pixel independently. It uses estimated value of the phase shift in this first stage.

In the second stage, it uses all pixels to calculate a correction of the phase shift estimation. This corrected estimation is then used in the next iteration [7].

3. Two-wavelength Interferometry

The measurement of the surface shape is complicated due to the problem of interferometry phase ambiguity. As the measured phase is contained in the range ⟨-π;+π⟩, the optical path difference (OPD) for one point is known in the range of $\lambda/2$.

Although some methods can be used to overcome ambiguity problem using surrounding points, some objects do not allow for this methods to be used. Typical examples of the problematic surfaces are surfaces with great slopes, discontinuities, and steps. As a result of the ambiguity, the step size is limited by the wavelength used.

Two-wavelength interferometry is based on measuring data at two known wavelengths. When two-wavelength interferometry is used, measureable step height is no longer limited by the wavelength of the used light but it is limited by a synthetic wavelength which can be calculated by means of function (8) from the two values of the wavelengths λ_1 and λ_2.

$$\lambda_s(\lambda_1, \lambda_2) = \frac{\lambda_2 \cdot \lambda_1}{|\lambda_2 - \lambda_1|} \quad (8)$$

The input of the synthetic phase evaluation algorithm is the product of phase shifting evaluation without unwrapping. The measured phases $\Delta\phi_i(x, y)$ form a phase map for a wavelength with the index i. Each phase map can be converted to the complex domain using expression (9).

$$\widehat{U}_i(x,y) = e^{i\cdot\Delta\phi_i} \tag{9}$$

To combine the phases of the two-wavelengths, expression (10) is used [9].

$$\widehat{U}_{ab}(x,y) = \widehat{U}_a(x,y)\cdot\left(\widehat{U}_b(x,y)\right)^* \tag{10}$$

An argument of the result complex number is the phase $\Delta\phi_{ab}$ of the synthetic wavelength.

$$\Delta\phi_{ab}(x,y) = \arg\left(\widehat{U}_{ab}(x,y)\right) \tag{11}$$

An optical path difference Δl_{ab} is calculated using expression (12).

$$\Delta l_{ab} = \frac{\Delta\phi_{ab}}{2\cdot\pi}\cdot\lambda_s(\lambda_a,\lambda_b) \tag{12}$$

The OPD has to be divided by 2 to obtain the measured surface height as the object wave has to travel the distance twice.

4. High Dynamic Range

Complex surfaces with different properties can provide very different reflectance in different areas. Visibility (14) of the interferometry fringes is given by the irradiance of the reflected-object light and by the irradiance of the reference light. It can be derived from the interference function (13). The I_{obj} is the irradiance of the light from the object arm, the I_{ref} is the irradiance from the reference arm, while the I is the overall irradiance of the interference. The angle ϕ is the phase difference between the object and the reference wave. Vector r represents coordinates in space.

$$I(\vec{r}) = I_{obj}(\vec{r}) + I_{ref}(\vec{r}) + 2\cdot\sqrt{I_{obj}(\vec{r})\cdot I_{ref}(\vec{r})}\cdot\cos(\phi) \tag{13}$$

$$v = \frac{2\cdot\sqrt{I_{obj}\cdot I_{ref}}}{I_{obj}+I_{ref}} \tag{14}$$

The highest visibility of the fringes is achieved when the irradiance of the reference and the object light reflected from the surface are equal, which can be deduced from expression (15).

$$\frac{\partial v}{\partial I_{ref}} = \frac{I_{obj}\cdot\left(I_{obj}-I_{ref}\right)}{\sqrt{I_{obj}\cdot I_{ref}}\cdot\left(I_{obj}+I_{ref}\right)^2} = 0 \tag{15}$$

$$I_{obj} = I_{ref} \tag{16}$$

A visibility problem is demonstrated in Fig. 2 using a simulation based on function (14). Two different surfaces are assumed. One surface reflects ten times more light than the other.

It is obvious that optimal visibility cannot be achieved with a single intensity of the reference light. To compensate for this problem, two or more measurements are performed for two or more different reference intensities with different camera settings. The intensity of the reference light can be controlled for example by electronically controlled attenuator.

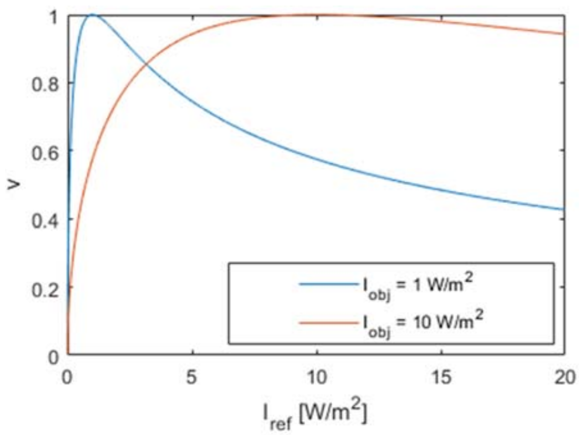

Fig. 2. Interference visibility for two different object arm irradiances as function of reference irradiance.

The data of the all measurements have to be merged together to perform the HDR. The evaluation algorithm need to decide which exposition setting is the optimal for each pixel. For this purpose, visibility values were calculated from the phase shifting amplitudes. A synthetic phase in each pixel is selected from the map in which the pixel has the highest visibility value.

A condition for the successful composition of the phase maps is that the phase δ at the beginning of each phase shifting sequence has to be the same. Alternatively, when it is not possible to ensure the same initial conditions, the phase difference has to be compensated during calculations. A source of the undesired phase shift can be for example the attenuator or a thermal dilatation of fibre line. If the undesired phase shift between each measurement is known it can be compensated in the calculations.

Function (4) describing phase shift during measurement can be altered to function (17) by adding the phase correction φ_c.

$$\bar{\delta}(t) = t\cdot\left(\omega_{obj}-\omega_{ref}\right)+\varphi_c \tag{17}$$

Function (5) can be altered to function (18) to compensate for the introduced phase shift φ_c.

$$\Delta\bar{\phi} = \arctan\left(\frac{I_4-I_2}{I_1-I_3}\right) - \varphi_c \tag{18}$$

The function (18) is then used to calculate the proper phase. It is then used as input to expression (9).

5. Experimental Device

In order to develop and test the improvement methods, an experimental holographic microscope was built.

5.1. The Device Assembly

In order to allow phase shifting using AOM and one arm attenuation, the fibre line topology in Fig. 3 was used.

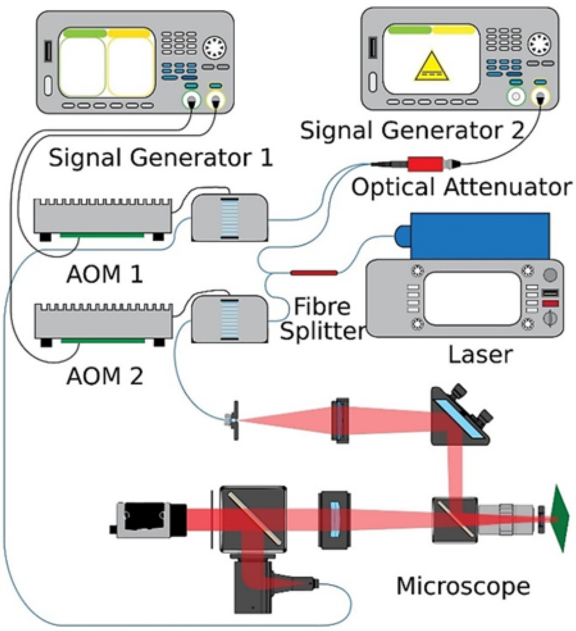

Fig. 3. Scheme of fibre lines topology.

A proposed topology of the microscope is presented in Fig. 4. It was decided to use epi-illumination [10] via a microscope objective, as it is intended to be used to inspect opaque samples.

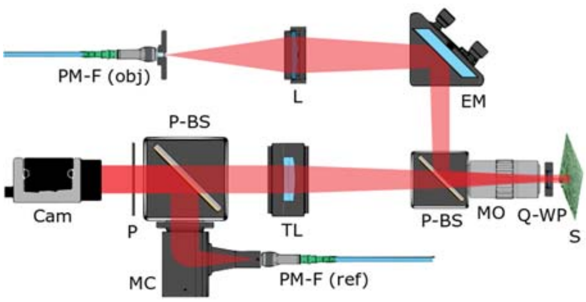

Fig. 4. The experimental microscope scheme. PM-F – PM Fibre, L – Lens, EM – Elliptic Mirror, P-BS – Pellicle Beam Splitter, MO – Microscope Objective, Q-WP – Quarter Wave Plate, S – Sample, TL – Tube Lens, MC – Mirror Collimator, P – Polarizer, Cam – Camera.

The photo of the finished device is presented in Fig. 5.

The device is equipped with the Mitutoyo MY5X-802 (5×) microscope objective and a linear actuator to bring a sample into focus. The object-illumination wavefront is introduced through a side tube and it is focused to a focal point of the microscope objective. Thus, the object-illumination beam passing via the objective forms collimated illumination.

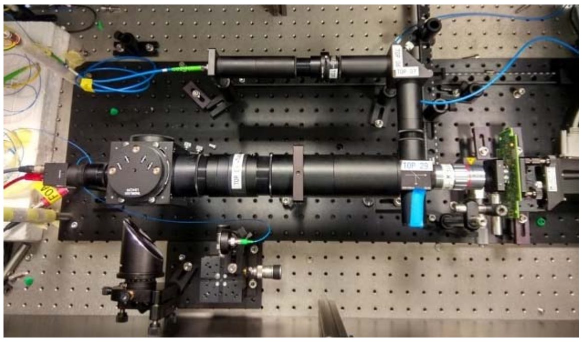

Fig. 5. The experimental holographic microscope.

The reference beam is collimated using a fibre collimator and reflected to a camera detector via a beam splitter. Light is brought to the device via polarization maintaining optical fibres. The supplied light has linear polarization. In order to reduce internal reflections inside the system, a quarter-wave plate was added between the microscope objective and the sample. This quarter-wave plate converts the linearly polarized illumination light to a circularly polarized light. A light reflected from the sample is converted back to linear polarization but it is rotated by 90° relatively to the light introduced to the system. A polarizer filter is placed in front of the camera to select specifically the polarization of the light reflected from the sample.

A Toptica DL pro 633 grating stabilised tuneable single-mode diode laser with a wavelength range from 631 nm to 635 nm was used as the coherent light source.

Each arm of the interferometer passes through one MT80-B16-R40-Fio-PM acousto-optic modulator which allows controlling output wavelength. A photo of the used AOM is shown in Fig. 6.

Fig. 6. One of the used AOM MT80-B16-R40-Fio-PM.

5.2. Attenuator Calibration

The intensity of the reference light is controlled using an electronically controlled attenuator V450PA in the reference arm. A condition for the successful composition of the phase maps is that the phase δ at the beginning of each phase shifting sequence has to be the same. Alternatively, when it is not possible to ensure the same initial conditions, the phase difference has to be compensated during calculations. For this reason, the phase of the AOM control signal was synchronised before each measurement to make the conditions identical. Nevertheless, it was discovered during measurement that the attenuator used in the reference arm introduces different phase shifts for different attenuation levels. This behaviour was measured using a simple experiment. The phase of the attenuator was measured for the different voltages of the control signal and a calibration curve was created. The calibration curve is plotted in Fig. 7.

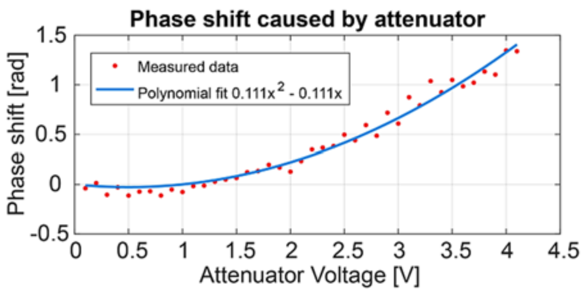

Fig. 7. The calibration curve of the V450PA attenuator.

6. Measurement Procedure

The measurement procedure consists of several steps. First, one of the two wavelengths is tuned on the tuneable laser. In the second step, the camera and the attenuator are configured for the first chosen reflectivity. The frequency of the control signal of the reference AOM is set to the value of f_{ref}. The frequency of the control signal of the object AOM is set to the value of f_{obj}. Both the control signals are synchronised to match phase and measurement is started immediately. A sequence of 13 frames with $\pi/4$ rad spacing is recorded. The camera and the attenuator are then configured for the next reflectivity. The AOMs are synchronised again and a sequence of 13 frames is recorded. The laser is then tuned to the next wavelength and the measurement procedure is repeated for the new wavelength. Whole measurement procedure and data evaluation is visualized in the diagram in Fig. 8.

7. Experimental Measurement

In order to test proposed measurement method, an experimental measurement was carried out.

7.1. Sample for the Measurement

As the sample for this measurement solution, a piece of PCB was chosen. PCB is a challenging sample as it has different layers with thickness higher than the used wavelength. The layers have great slopes on the edges and the surfaces have diverse diffusivity and reflectivity. It was chosen as a typical industrial product to be analysed. A part of the sample was painted with a thin layer of white paint to improve reflectivity. The used region on the PCB is marked in Fig. 9. The expected layer thickness is around 30 µm.

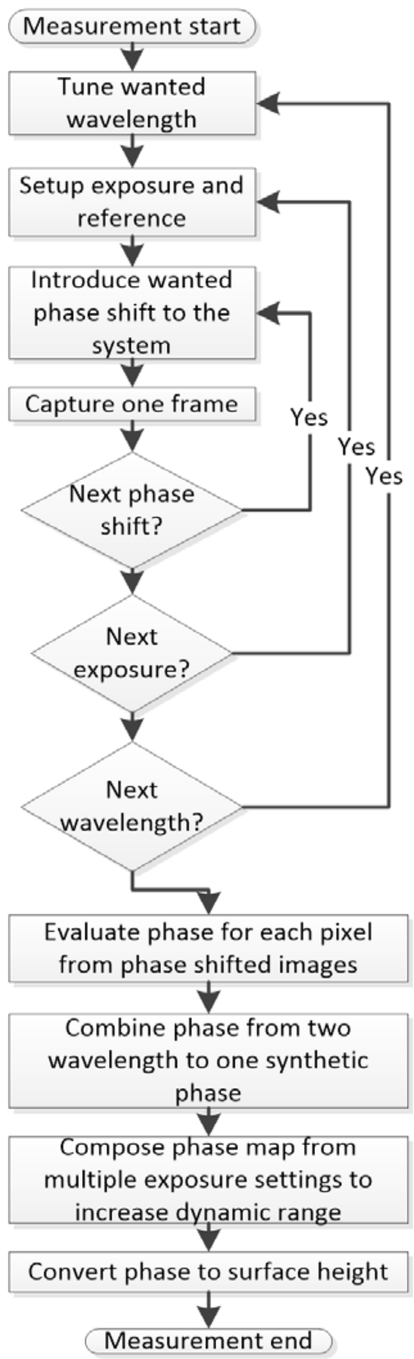

Fig. 8. State diagram of the measurement procedure and data evaluation.

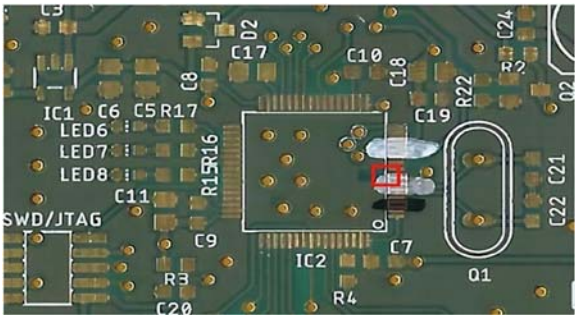

Fig. 9. The used sample with the measured area marked by a red rectangle.

7.2. Measurement Parameters

The parameters of the measurement are presented in Table 1.

Table. 1. Parameters of the experimental measurement. Table contains

Parameter	Value	Description
f_{ref}	80,000,000 Hz	Control signal frequency for AOMs
f_{obj}	80,000,001 Hz	
λ_1	630.45 nm	Chosen wavelengths
λ_2	632.28 nm	
V_1	1 V	Attenuator voltages
V_2	3 V	
V_3	3.35 V	
F_S	8 Hz	Camera frame rate

The frequency of the acousto-optics modulators control signal was chosen to be close to the optimal frequency for the used wavelength. The difference between frequencies for the control signals was chosen to be 1 Hz. Frame rate of the camera was set to 8 Hz to get exactly eight samples per one period of the phase shift.

The presented experimental data were measured at two different wavelengths of 630.45 nm and 632.28 nm. Based on equation (8), it means that the synthetic wavelength was 218 µm. [9]. This wavelength is higher than the expected layer thickness of the PCB with a safety margin.

Three voltage levels for attenuator and three camera exposure setting were chosen to obtain data for HDR.

7.3. Evaluated Data

The captured intensity images for each attenuator setting are presented in Figs. 10, 11 and 12.

The Thirteen steps algorithm was used to get phase. In Fig. 13, pixels are marked by colour to illustrate from which intensity setting the phase values were taken.

Phase data converted to a height map are displayed in Fig. 14.

The solution provides fine lateral resolution (around 0.7 µm) and vertical precision. The thickness of each layer can be measured with this solution.

7.4. Uncertainty and Noise Analysis

It can be observed that areas where the surface is not covered with any layer or paint are very noisy. This phenomenon is probably caused by the properties of the base material of the PCB.

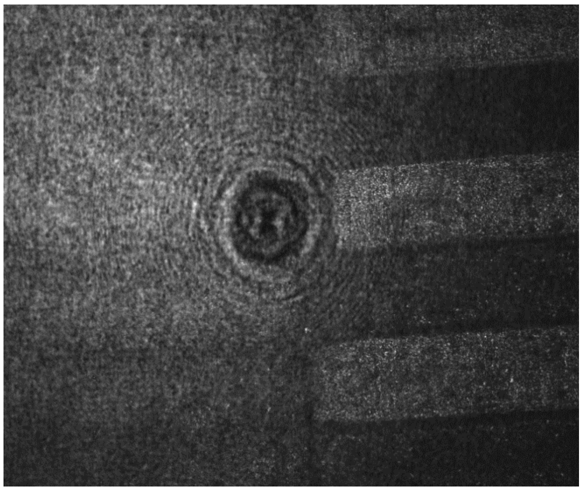

Fig. 10. An intensity image captured by the camera for the lowest attenuation in the reference arm. The control voltage was 1 V.

Fig. 11. An intensity image captured by the camera for the lowest attenuation in the reference arm. The control voltage was 3 V.

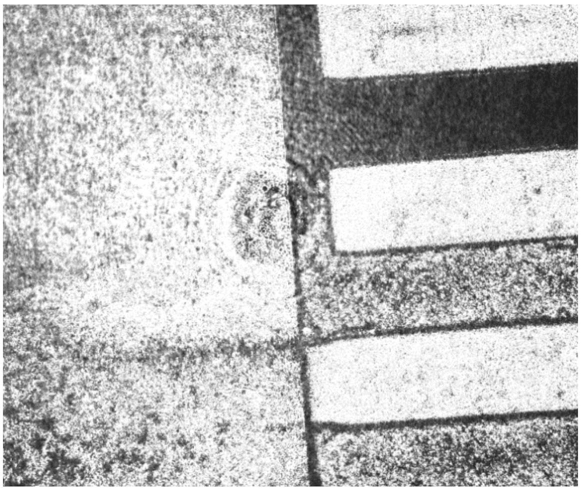

Fig. 12. An intensity image captured by the camera for the lowest attenuation in the reference arm. The control voltage was 3.35 V.

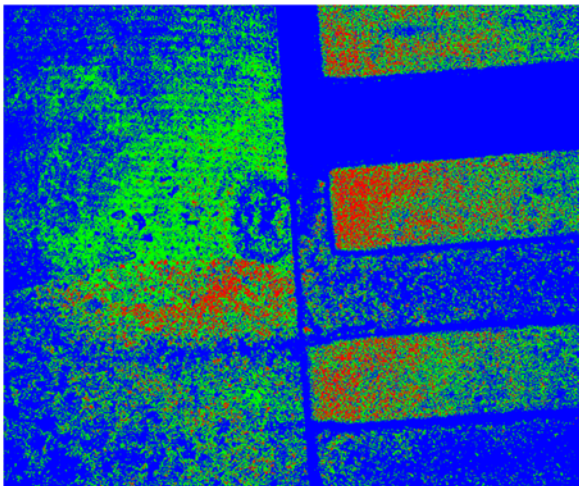

Fig. 13. A colour map of contribution in the composed data. Red areas are for the lowest reference arm attenuation, green areas are for medium attenuation and blue areas are for the highest attenuation.

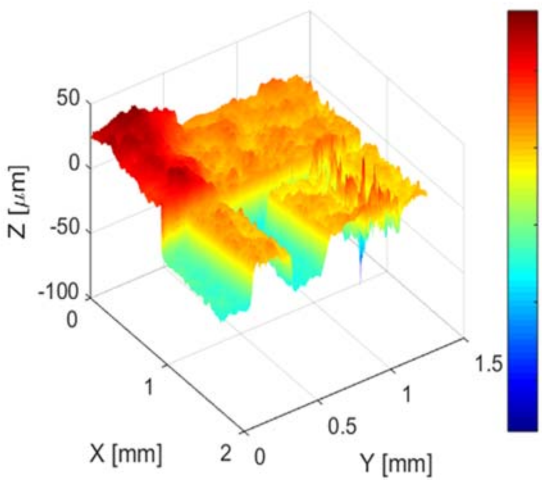

Fig. 14. The measured height map of the chosen area on the PCB.

The base material is semi-transparent and semi-absorbent, which could be a problem for the phase evaluation.

In order to evaluate impact of the proposed HDR method, one height map was processed from the data measured with the lowest attenuation in reference arm and with the lowest camera exposure. This measurement was chosen from the dataset because it is able to provide information from all parts without saturation. It can be observed in Fig. 15, that the noise level in the areas with lower reflectivity is higher without HDR.

Both presented results were filtered with a weighting filter of size 50 × 50 px. The modulation amplitude was used as the weight for the filtration.

A small area of the lower part of the PCB was selected to be used for a statistical noise analysis. The area is marked in Fig. 16.

The selected area for the data processed with the HDR method are visualized in Fig. 17. The selected area for the data processed without the HDR method are visualized in Fig. 18.

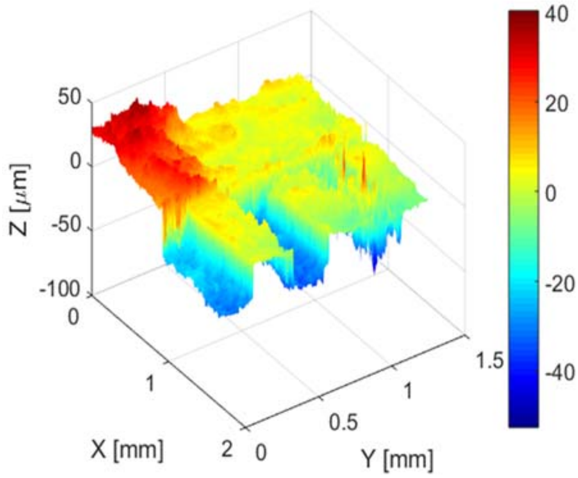

Fig. 15. The measured height map evaluated without the HDR from the measurement with the lowest attenuation.

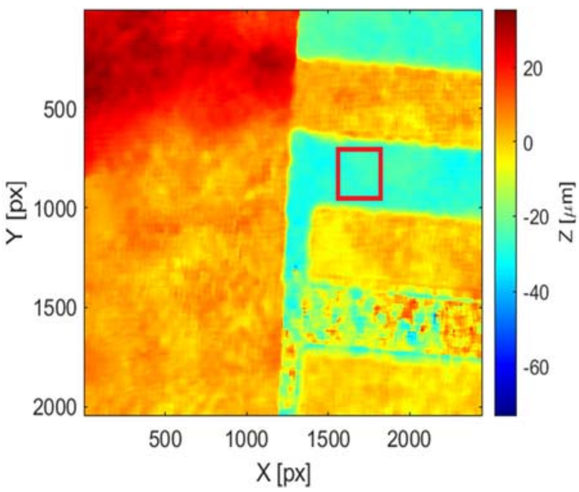

Fig. 16. The valuated data with the marked area to be used for HDR effect evaluation.

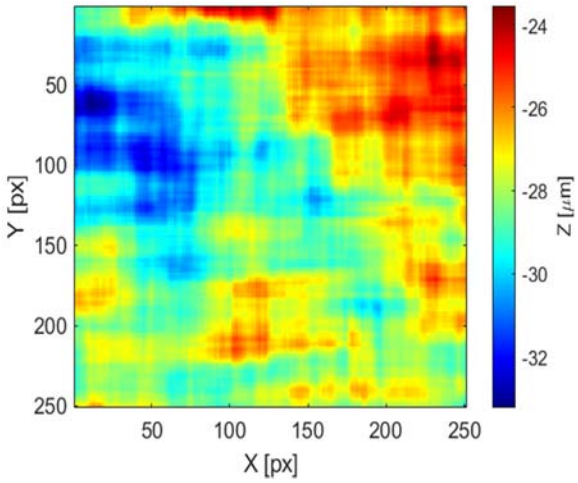

Fig. 17. A selection of the data processed from three intensity measurement.

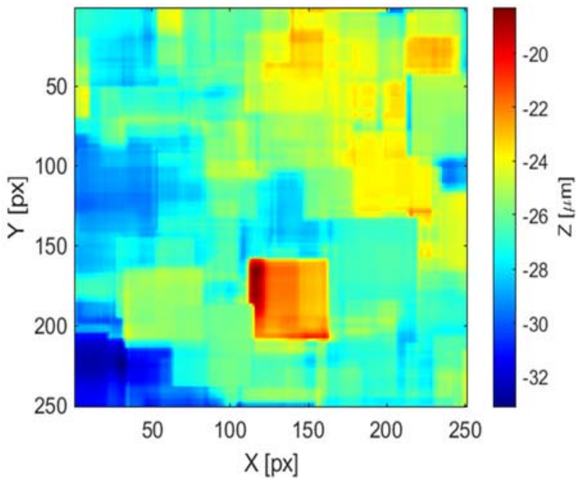

Fig. 18. A selection of the data processed from one intensity measurement.

The both cropped areas were pre-processed first by removing a tilt and a piston. Noise level was evaluated as root mean square (RMS) for the data processed with the HDR and without the HDR and compared. The RMS values were calculated using following expression.

$$RMS = \sqrt{\frac{\sum_{i=1}^{M}\sum_{j=1}^{N} Z[i,j]^2}{M \cdot N}} \quad (19)$$

The data processed without HDR have the RMS 1.6539 μm and the data from three intensities with applied HDR have RMS 1.2239 μm. It means that the HDR method reduces the noise in the chosen area by 26 %.

The vertical precision of the measurement method is influenced by many factors. The factor which limits the measurement precision the most is the noise. When the noise is reduced, the overall precision is increased.

8. Comparison with Other Measurement Methods

For comparison reasons, the chosen area on the PCB was measured with a Zygo NewView™ 7200 white light interferometer. The data are presented in Fig. 19. It is noticeable that the surface measured by the Zygo device was able to provide more useful information of the areas where the paint was not applied. Nevertheless count of the valid pixel is lower than in the areas where paint was applied. The data measured with the Zygo device are distorted to different shape if compared with the data measured with the developed device.

9. Conclusions

The assembled experimental device and the performed experiment helped to verify the theoretical principles of DHM. A measurement procedure enhancement to increase dynamic range was devised and tested. An innovative way of inducing the phase shift using an AOM was tested. The measured data confirmed that the AOM is very stable and can be used as a precise metrological-grade way of phase shifting.

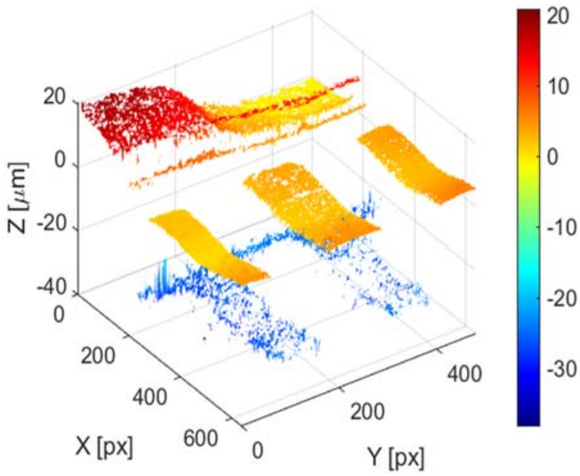

Fig. 19. The height map of the chosen area on the PCB measured by a Zygo white light interferometer.

It was discovered that the used attenuator has a variable phase delay as a function of the control voltage. This behaviour is problematic when the phase data from multiple different measurements need to be composed. A solution based on the calibration and computational compensation was proposed and used.

The measured data were used to test and develop data evaluation algorithms. Especially, algorithms for two-wavelength interferometry, phase evaluation, and HDR were developed.

Although this solution was unable to measure some parts of the PCB sample, it could be feasible to inspect the sample when a thin layer of paint is applied. With this treatment, the measurement method can be used for PCB inspection when a production technology needs to be optimised.

The noise level was evaluated for data processed with and without the HDR method. The results indicated 26 % improvement of the noise value.

The device measurement capabilities were compared with the commercial device Zygo NewView™ 7200. The developed device was able to provide the 3D image of the sample surface without the shape distortion.

Acknowledgements

This work was supported by the Student Grant Scheme at the Technical University of Liberec through project No. SGS-2019-3050.

Authors acknowledge the support from the Czech Science Foundation (project number GACR 19-22000S).

References

[1]. D. Carl, B. Kemper, G. Wernicke, G. V. Bally, Parameter-optimized digital holographic microscope for high-resolution living-cell analysis: *Applied Optics*, Vol. 43, Issue 36, 2004, pp. 6536-6544.

[2]. P. Marquet, B. Rappaz, P. J. Magistretti, E. Cuche, Y. Emery, T. Colomb, Christian Depeursinge, Digital holographic microscopy: a noninvasive contrast imaging technique allowing quantitative visualization of living cells with subwavelength axial accuracy, *Optics Letters*, Vol. 30, Issue 5, 2005, pp. 468-470.

[3]. V. R. Singh, C. Gorecki, A. K. Asundi, A. Andrei, W. Osten, L. Nieradko, Characterization of MEMS cantilevers using lensless digital holographic microscope, *Proc. SPIE 6995, 2008, SPIE Photonics Europe*, Strasbourg, France, 2008.

[4]. D. Parshall, M. K. Kim, Digital holographic microscopy with dual-wavelength phase unwrapping, *Applied Optics*, Vol. 45, Issue 3, 2006, pp. 451-459.

[5]. A. Asundi, Digital Holography for MEMS and Microsystem Metrology, *John Wiley and Sons*, *Ltd*, 2011.

[6]. M. Stašík, F. Kaván, M. Mach, K Sedláčková, J. Kredba, M. Špína, Two-wavelengths Interferometry as Confocal Microscope Extension to Provide 3D Imaging Capabilities, in *Proceedings of the 3rd International Conference on Optics, Photonics and Lasers (OPAL'2020)*, Tenerife (Canary Islands), Spain, 21-23 October 2020, pp. 20-25.

[7]. I. Kong, S. Kim, General algorithm of phase-shifting interferometry by iterative least-squares fitting, *Optical Engineering*, Vol. 34, Issue 1, 1995.

[8]. T. Kreis, Handbook of Hologhraphic Interferometry, *Wiley-VCH*, 2005.

[9]. V. Lédl, P. Psota, P. Vojtíšek, R. Doleček, P. Mokrý, Holographic contouring and its limitations in nearly specularly reflecting surface measurement, in *Proceedings of the Optics and Measurement Conference*, Proc. SPIE 9442, 2014, 94420Q, 2015.

[10]. ZEISS Microscopy Online Campus | Microscopy Basics | Illumination and the Optical Train (http://zeiss-campus.magnet.fsu.edu/articles/basics/opticaltrain.html)